Available online at www.sciencedirect.com
ScienceDirect
Thermochimica Acta 460 (2007) 22–27
thermochimica acta
www.elsevier.com/locate/tca

Isothermal and non-isothermal melting of the binary solution inside an emulsion

A. Jamil, T. Kousksou *, Y. Zeraouli, J.-P. Dumas, E. Schall

Laboratoire de Thermique Énergétique et Procédés, Avenue de l'Université, BP 1155, 64013 PAU CEDEX, France

Received 14 March 2007; received in revised form 30 April 2007; accepted 1 May 2007
Available online 6 May 2007

Abstract

The aim of the present paper is to study the melting process inside an emulsion using the non-equilibrium model of microscopic heat transfer between the emulsifying medium and the dispersed droplet of binary solution (DSC). DSC experiments are used to validate the numerical results. The effects of the heating rate, mass fraction of the dispersed saline binary solution, initial mass fraction of the solute and the sample mass on the kinetics of the melting process are examined.

Keywords: Heat transfer; Ammonium chloride; Emulsion; DSC; Thermodynamics

1. Introduction

Emulsions are the subject of several studies in the recent literature. Much of this work is concentrated upon the caracterizing of the emulsion morphology and the effects of some parameters on it [1,2].

Our research group worked for a long time on the heat transfer during crystallization or melting within an emulsion. We have presented some models concerning the heat transfer in the case of a phase change of binary solutions dispersed within emulsions or micro-emulsions (see Refs. [3–6]).

To obtain more information about the kinetics of the eutectic and progressive melting of the crystallized droplets dispersed inside emulsion, we have developed a non-equilibrium model taking into account the interphase heat transfer between the emulsifying medium and the dispersed droplet. The effects of the heating rate, mass fraction of the dispersed saline binary solution, initial mass fraction of the solute and the sample mass on the kinetics of the melting process are investigated.

2. Equilibrium phase diagram of binary system

Fig. 1 shows the equilibrium phase diagram for the NH_4Cl–H_2O system. The symbols L, S and L + S denote the liquid phase, the solid phase and the solid–liquid two-phase, respectively.

The lowest temperature possible for liquid salt solution is −15.7 °C. At that temperature, the salt begins to crystallize out of solution, along with the ice, until the solution completely freezes. The frozen solution is a mixture of separate solute crystals and ice crystals. This mixture is called a eutectic mixture. If the ice, salt and the saltwater are present in the binary mixture, and their amounts are not changing over time we must be at the eutectic point ($T_E = -15.7\,^{\circ}C$ and $X_E = 0.195$).

In our application, the over-eutectic part is not of interest. If the solute mass fraction X_a is lower than X_E the ice mass fraction X_{ic} can be calculated from the liquidus temperature of the binary mixture solution, which is a function of X_a.

$$T = T(X_a) \tag{1}$$

Once the initial mass fraction of solute in the binary mixture solution before freezing $X_{a,i}$ and temperature are known, the equilibrium ice mass fraction is calculated with:

$$X_{ic}(T) = 1 - \frac{X_{a,i}}{X_a(T)} \tag{2}$$

in which $X_a(T)$ is found from the liquid curve, the inverse of Eq. (1).

* Corresponding author.
E-mail address: Tarik.kousksou@univ-pau.fr (T. Kousksou).

0040-6031/$ – see front matter © 2007 Elsevier B.V. All rights reserved.
doi:10.1016/j.tca.2007.05.004

Nomenclature

c	specific heat ($J\,kg^{-1}\,K^{-1}$)
h	exchange coefficient for the droplet ($W\,m^{-2}\,K^{-1}$)
h_1, h_2	external exchange coefficient for the cell ($W\,m^{-2}\,K^{-1}$)
k	thermal conductivity ($W\,m^{-1}\,K^{-1}$)
L_D	heat of dissolution of salt in the solution ($J\,kg^{-1}$)
L_F	latent heat of melting of the ice ($J\,kg^{-1}$)
P	mass fraction of the dispersed solution
ΔS	area (m^2)
t	time (s)
T	temperature (K)
X_E	eutectic concentration
X_{ic}	ice mass fraction
X_g	ice mass fraction which is melted

Greek symbols

β	heating rate ($K\,min^{-1}$)
ρ	mass density ($kg\,m^{-3}$)
ε	porosity
Φ	specific heat flow rate ($W\,kg^{-1}$)

Subscripts

a	antifreeze
em	emulsion
f	emulsifying medium
i	initial
ic	ice
s	solution

3. Formulations

Thermal analysis was carried out using a PYRIS DIAMOND DSC of Perkin-Elmer. The temperature scale of the instrument was calibrated by the melting point of pure ice (273.15 K or 0 °C) and mercury (234.32 K or −38.82 °C). The principle of the power-compensation used in dispersed droplet of binary solution (DSC) is widely detailed in Refs. ([7,8]).

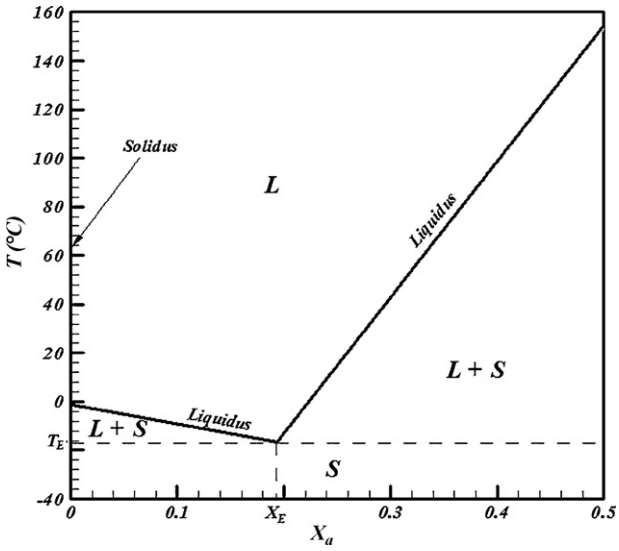

Fig. 1. Phase diagram for a binary solution (NH_4Cl–H_2O).

In Fig. 2, we have drawn the real cell and the simplified scheme used in our model. The emulsion fills a cylindrical cell of height $Z_0 = 1.1$ mm and radius $R = 2.125$ mm.

To study the melting process inside an emulsion, we assume that the emulsifying medium and the droplets are not in local thermodynamic equilibrium and, therefore, a two-temperature model of microscopic heat transfer applies. The governing equations for the emulsifying medium and the solution temperatures are:

$$\varepsilon(\rho c) f \frac{\partial T_f}{\partial t} = \varepsilon k_f \nabla^2 T_f + h(T_s - T_f) \tag{3}$$

$$(1-\varepsilon)(\rho c)_s \frac{\partial T_s}{\partial t} = h(T_f - T_s) \tag{4}$$

where T is the temperature, ρ the mass density, c the specific heat, k the thermal conductivity, h the overall constant heat transfer coefficient, f and s subscripts denote the emulsifying medium and solution phases, respectively, and ε is the porosity defined by the following relation:

$$\varepsilon = 1 - P\frac{\rho_{em}}{\rho_s} \tag{5}$$

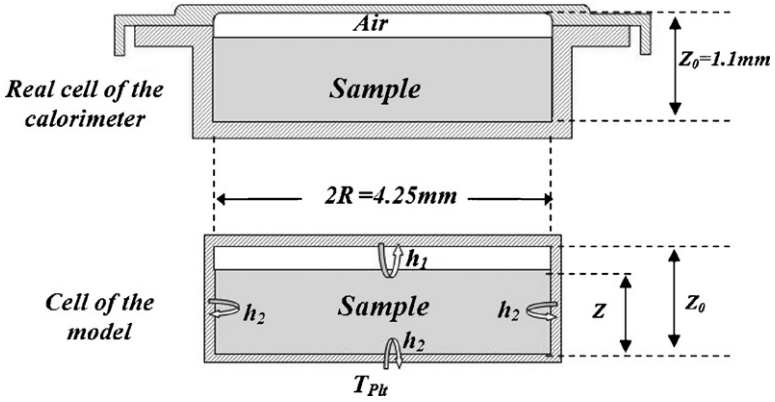

Fig. 2. Experimental cell and scheme for the model.

where P is the ratio between the mass of the dispersed solution and the mass of the emulsion and ρ_{em} is the mass density of the emulsion.

During the isothermal melting (i.e., eutectic melting), the energy balance is quite different because $T_s = T_E$ and the exchanged heat proceeds from the fraction of crystal which is melting:

$$(1-\varepsilon)\rho_{ic}A\frac{\partial X_{ic}}{\partial t} = -h(T_f - T_E) \quad (6)$$

X_{ic} indicates the ice mass fraction. The coefficient A is given by:

$$A = L_F(T) + \frac{X_E}{1-X_E}L_D \quad (7)$$

where L_F and L_D represents the latent heat of fusion of ice and the dissolution heat of salt in the formed solution, respectively.

During the non-isothermal melting (i.e., progressive melting), the appropriate equation for the eutectic mixture is

$$(1-\varepsilon)\rho_s c_s\frac{\partial T_s}{\partial t} = (1-\varepsilon)\rho_{ic}L_F\frac{\partial X_{ic}}{\partial t} + h(T_f - T_s) \quad (8)$$

In the above equation, the unknowns are only the temperatures T_s because the ice mass fractions X_{ic} are themselves function of the temperatures according the Eq. (2) (see Ref. [8]).

To take into account the air between the sample and the cover of the cell, we consider two different heat exchange coefficient h_1 and h_2. So, the boundaries conditions are:

$$\left(\frac{\partial T}{\partial r}\right)_{r=0} = 0 \quad (9)$$

$$-k_f\left(\frac{\partial T}{\partial r}\right)_{r=R} = h_2(T - T_{plt}) \quad (10)$$

$$-k_f\left(\frac{\partial T}{\partial z}\right)_{z=0} = h_2(T - T_{plt}) \quad (11)$$

$$-k_f\left(\frac{\partial T}{\partial z}\right)_{z=Z} = h_1(T - T_{plt}) \quad (12)$$

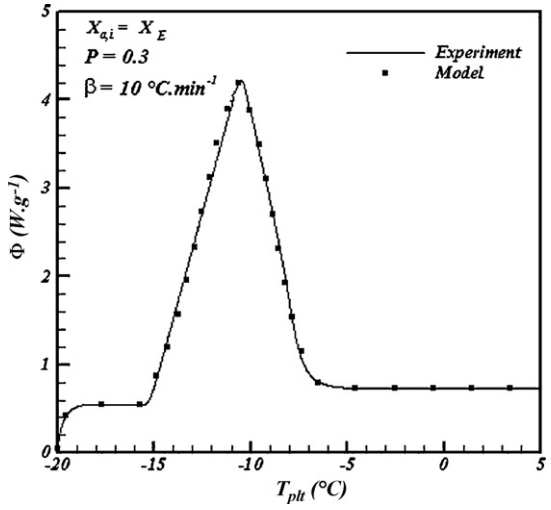

Fig. 3. Theoretical and experimental thermogram ($X_{a,i} = X_E$, $\beta = 10\,^{\circ}\mathrm{C\,min^{-1}}$, $P = 0.3$).

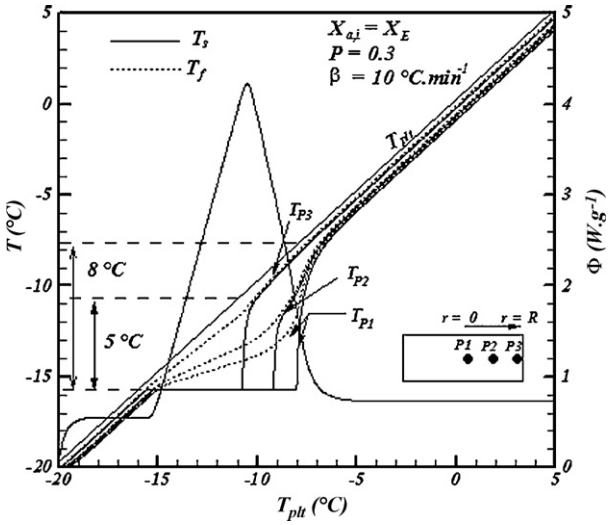

Fig. 4. T_f and T_s vs. radius r ($X_{a,i} = X_E$, $\beta = 10\,^{\circ}\mathrm{C\,min^{-1}}$, $P = 0.3$).

where T_{plt}, the temperature of the plates, is programmed to be linear function

$$T_{plt} = \beta t + T_0 \quad (13)$$

At $t = 0$ the initial conditions are $T(r,z,0) = T_0$ and $X_{ic}(r,z,0) = 0$ or $X_g(r,z,0) = 1 - X_E$.

Because the thermal conductivity of air is smaller than that of the metal of the cell, we consider that all the energy is transmitted to the plate by the lower boundary of the cell. So, Φ is the sum of the thermal fluxes through the walls of the metallic cell

$$\Phi = -\sum_i h_i(T_i - T_{plt})\Delta S_i \quad (14)$$

where $h_i = h_1$ or h_2.

4. Results and discussion

The values of physical characteristics required in different equations have been determined experimentally or using the lit-

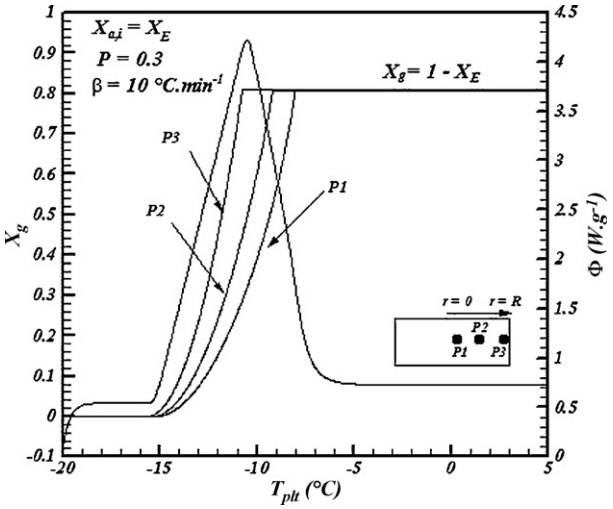

Fig. 5. X_g vs. radius r ($X_{a,i} = X_E$, $\beta = 10\,^{\circ}\mathrm{C\,min^{-1}}$, $P = 0.3$).

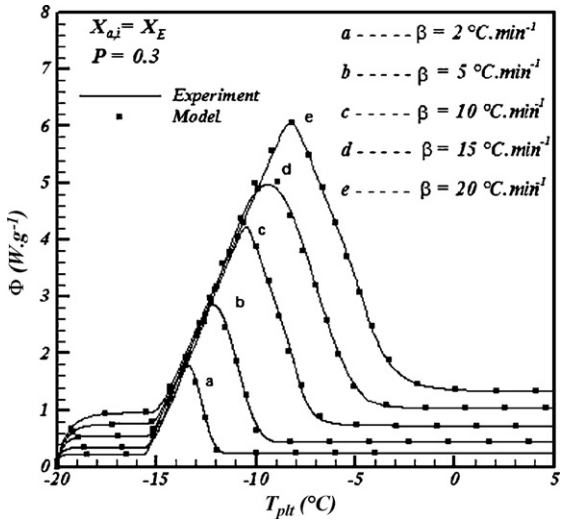

Fig. 6. Effect of the heating rate on the shape of thermograms for $X_{a,i} = X_E$.

erature correlations [9], except the coefficients of heat exchange (h_1, h_2 and h) that have been determined by simulation from exploratory experiments.

4.1. The case for $X_{a,i} = X_E$

Fig. 3 illustrates the experimental thermogram for the eutectic melting ($X_E = 0.195$, $T_E = -15.7\,^\circ C$), at $10\,^\circ C\,min^{-1}$, compared with the theoretical thermogram obtained with the proposed model. Naturally, no two-phase region emerges for $X_{a,i} = X_E$ and the shape of the thermogram is similar to that for ordinary pure liquids. The fit between the experimental and the calculated curves is good: the rounded form of the top of the peak is reproduced and its width is the same.

Figs. 4 and 5 present the temperatures T_f, T_s and the corresponding ice mass fraction which is melted X_g at different points of the cell versus T_{plt}. Important temperature differences can be observed as a function of the radius or the height of the cell. These differences can reach 6 °C. There is a small difference

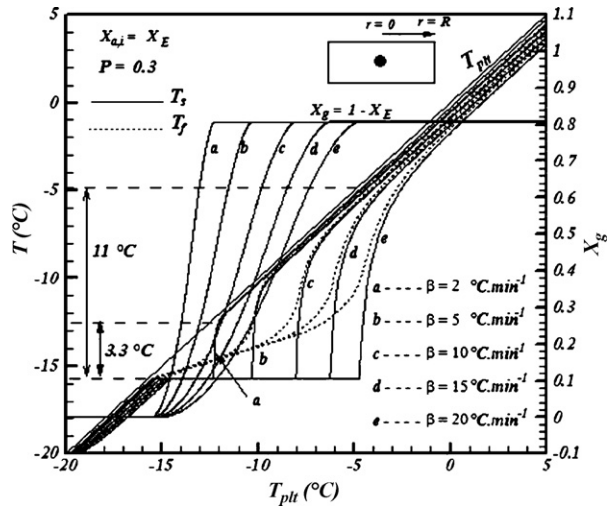

Fig. 7. Effect of the heating rate β on T_f, T_s and X_g in the center of the sample.

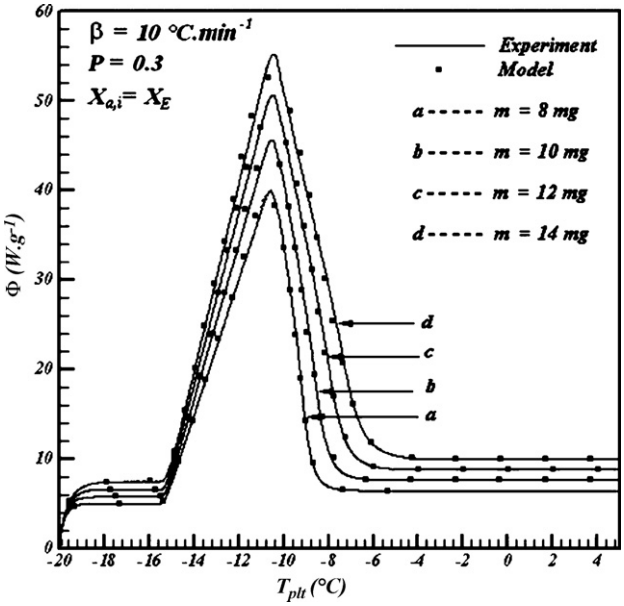

Fig. 8. Influence of the sample mass on the shape of thermograms.

between the temperature of the emulsifying medium and the inner temperature of the binary solution.

Fig. 6 shows the thermograms obtained by the model and DSC versus the heating rate β. The melting temperatures range becomes broader and it shifts to greater temperature with increasing heating rate. We can note that the peak maximum temperature T_{peak} increases continuously with increasing heating rate. This effect on the peak temperatures is caused by the thermal resistance between the sample and the DSC plate form.

Fig. 7 displays the prediction of temperatures T_f, T_s and the corresponding ice mass fraction which is melted X_g versus T_{plt} in the center of the sample for different heating rate. It can be seen from this figure that the temperature differences inside the sample becomes more important as the heating rate increases.

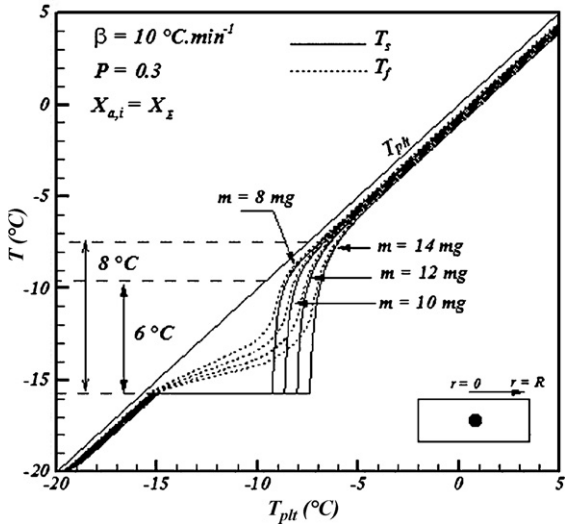

Fig. 9. Effect of the sample mass on T_f and T_s in the center of the sample ($\beta = 10\,^\circ C\,min^{-1}$, $P = 0.3$).

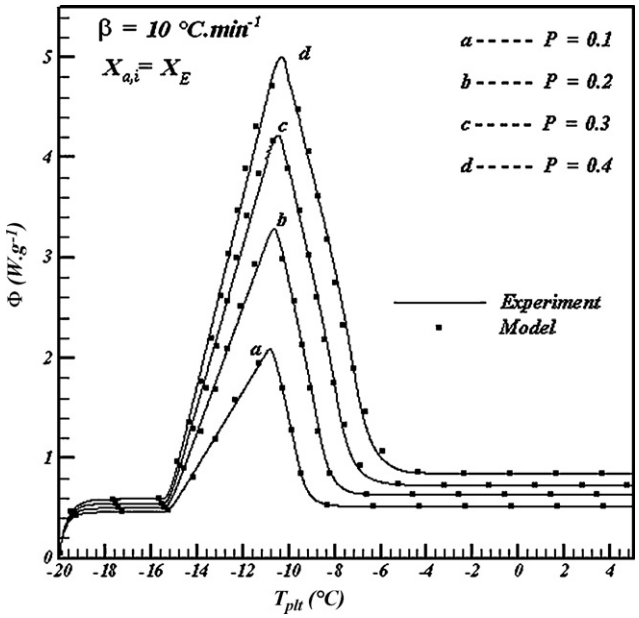

Fig. 10. Influence of the mass fraction P on the shape of thermograms.

From the numerical and experimental analysis, we can present the non-normalized heat flow for different mass of the sample at a fixed heating rate, as one can see in Fig. 8. In these plots we found that the peak temperature increases with increasing the mass of sample.

In Fig. 9, we observe that the temperature difference inside sample becomes more important as the mass of sample increases.

In Fig. 10, we have plotted curves giving the experimental and theoretical thermograms versus the mass fraction P. We can note that the kinetics of the melting process depends on P.

4.2. The case for $X_{a,i} \prec X_E$

For each initial mass fraction of the solute we have traced experimental and numerical heat flow (see Fig. 11). The thermograms exhibit isothermal eutectic and non-isothermal

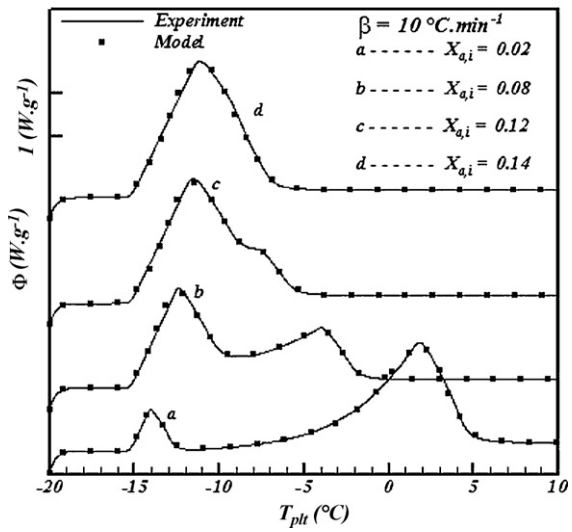

Fig. 11. Thermograms for different concentrations.

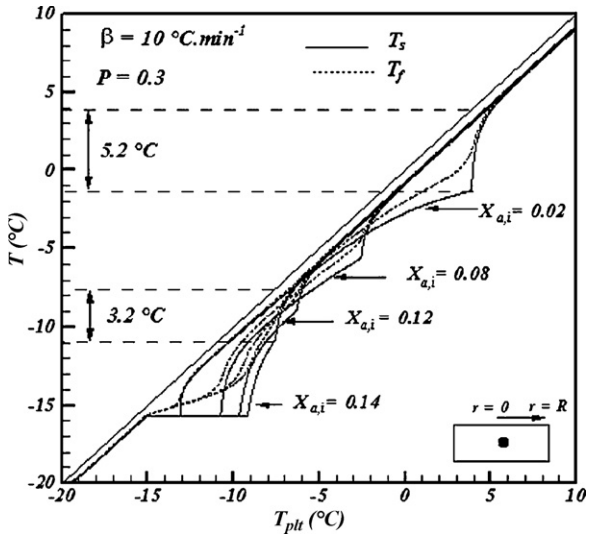

Fig. 12. Effect of $X_{a,i}$ on T_f and T_s in the center of the sample ($\beta = 10\,^{\circ}\mathrm{C\,min^{-1}}$, $P = 0.3$).

solid–liquid transition peaks. We note that the peak temperature of the progressive melting decreases with increasing initial mass fraction of the solute since the liquidus temperature decreases (Fig. 1). When the initial mass fraction of the solute is much smaller than the eutectic concentration, the amount of the ice transformed during the eutectic melting is very little.

Figs. 12 and 13 display the temperatures T_f, T_s and the corresponding ice mass fraction which is melted X_g in the center of the cell versus T_{plt}. We observe that the temperature difference inside sample becomes more important as the initial mass fraction of solute decreases.

Fig. 14 illustrates the numerical heat flow versus the heating rate for $X_{a,i} = 0.12$. We show that the peak corresponding to the eutectic melting becomes larger when the heating rate increases. Increase in β leads to the disappearance of the second peak. It

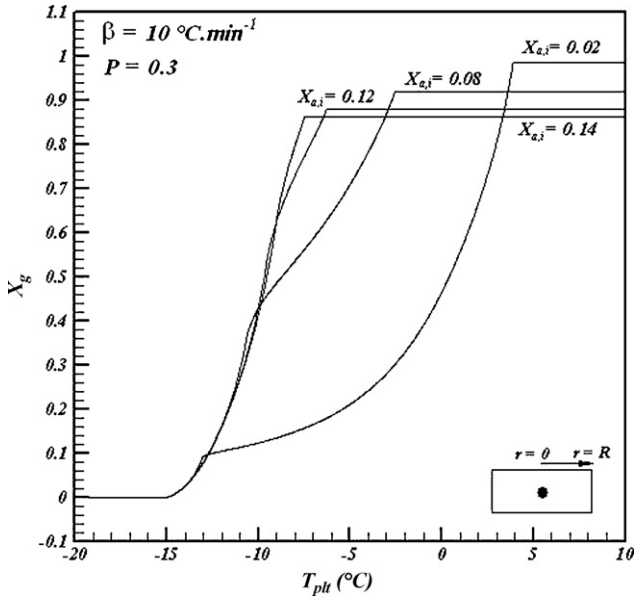

Fig. 13. Effect of $X_{a,i}$ on X_g in the center of the sample.

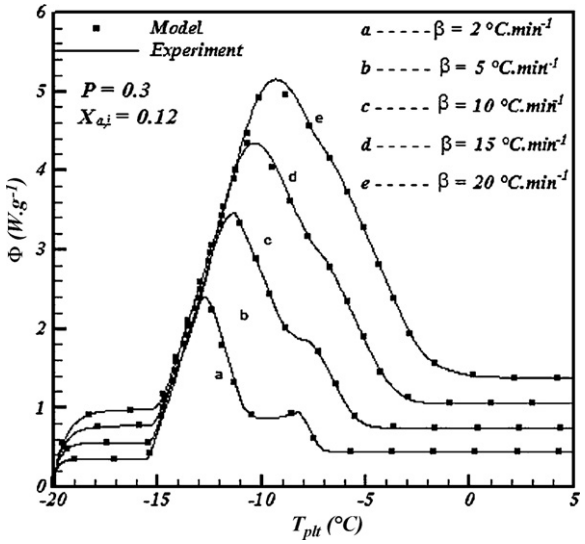

Fig. 14. Effect of the heating rate on the shape of thermogram for $X_{a,i} = 0.12$.

is clearly seen that the use of the high heating rate masque the essential information about the progressive melting.

5. Conclusion

The effects of the heating rate, mass fraction of the dispersed solution, sample mass and the initial concentration of the solute are systematically examined using dispersed aqueous ammonium chloride. It can be concluded that the use of the higher sample mass increases the temperature gradients in the emulsion. In order to describe with accuracy the heat transfer during the melting process inside emulsion, it is desirable to use the lower heating rate.

References

[1] D. Clausse, F. Gomez, I. Pezron, L. Komunjer, C. Dalmazzone, Morphology characterization of emulsions by differential scanning calorimetry, Adv. Colloid Interface 117 (2005) 59–74.
[2] J.L. Grossiod, Multiple Emulsions: Structure, Properties and Applications, Editions de Santé, Paris, 1998.
[3] J.P. Dumas, Y. Zeraouli, M. Strub, M. Krichi, Models for the heat transfers during the transformations inside an emulsion II. Melting of the crystallized droplets, Int. J. Heat Mass Transfer 37 (1994) 747–752.
[4] Y. Zeraouli, A.J. Ehmimed, J.P. Dumas, Modéles de transferts thermiques lors de la fusion d'une solution binaire dispersée, Int. J. Therm. Sci. 39 (2000) 780–796.
[5] S. Gibout, M. Strub, J.P. Dumas, Estimation of the nucleation probability in emulsions, Int. J. Heat Mass Transfer 47 (2004) 63–74.
[6] S. Gibout, A. Jamil, T. Kousksou, Y. Zeraouli, J. Castaing-Lasvignottes, Experimental determination of the nucleation probability in emulsions, Thermochim. Acta 441 (2006) 30–34.
[7] A. Jamil, T. Kousksou, S. Gibout, Y. Zeraouli, J.P. Dumas, Simulation of the thermal transfer during an eutectic melting of a binary solution, Thermochim. Acta 448 (2006) 129–132.
[8] T. Kousksou, A. Jamil, Y. Zeraouli, J.P. Dumas, DSC study and computer modeling of the melting process in ice slurry, Thermochim. Acta 448 (2006) 123–129.
[9] J. Timmermans, The Physico-Chemical Constants of Binary Systems in Concentrated Solutions, vol. 4, New York, 1960, pp. 123–129.